






Cerebral angiogenesis ameliorates pathological disorders in *Nemo*-deficient mice with small-vessel disease

Yun Jiang¹, Kristin Müller¹, Mahtab A. Khan¹ , Julian C. Assmann¹, Josephine Lampe^{1,2}, Knut Kilau^{1,2}, Marius Richter¹, Maximilian Kleint¹, Dirk A Ridder¹, Norbert Hübner^{2,3,4}, Marc Schmidt-Supprian⁵, Jan Wenzel^{1,2,*}  and Markus Schwaninger^{1,2,*} 

Abstract

Cerebral small-vessel diseases (SVDs) often follow a progressive course. Little is known about the function of angiogenesis, which potentially induces regression of SVDs. Here, we investigated angiogenesis in a mouse model of incontinentia pigmenti (IP), a genetic disease comprising features of SVD. IP is caused by inactivating mutations of *Nemo*, the essential component of NF- κ B signaling. When deleting *Nemo* in the majority of brain endothelial cells (*Nemo*^{beKO} mice), the transcriptional profile of vessels indicated cell proliferation. Brain endothelial cells expressed Ki67 and showed signs of DNA synthesis. In addition to cell proliferation, we observed sprouting and intussusceptive angiogenesis in *Nemo*^{beKO} mice. Angiogenesis occurred in all segments of the vasculature and in proximity to vessel rarefaction and tissue hypoxia. Apparently, NEMO was required for productive angiogenesis because endothelial cells that had escaped *Nemo* inactivation showed a higher proliferation rate than *Nemo*-deficient cells. Therefore, newborn endothelial cells were particularly vulnerable to ongoing recombination. When we interfered with productive angiogenesis by inducing ongoing ablation of *Nemo*, mice did not recover from IP manifestations but rather showed severe functional deficits. In summary, the data demonstrate that angiogenesis is present in this model of SVD and suggest that it may counterbalance the loss of vessels.

Keywords

Angiogenesis, small vessel disease, incontinentia pigmenti, NF- κ B, endothelial cell

Received 24 October 2019; Revised 23 January 2020; Accepted 29 January 2020

Introduction

Cerebral small-vessel diseases (SVDs) represent a frequent cause of stroke, dementia, mood disorders, and motor dysfunction, especially in the elderly.¹ The course of these diseases is mostly progressive, without showing any significant clinical regression.² So far, no therapy is available. Characteristic pathological changes in small vessels of the brain encompass lipohyalinosis and other changes in the wall of arterioles and a loss of capillaries.^{3–5} When endothelial cells (ECs) in cerebral capillaries die, the ensheathing basement membrane persists leading to the morphological structure of string vessels, also known as empty basement membrane tubes.⁵

¹Institute for Experimental and Clinical Pharmacology and Toxicology, University of Lübeck, Lübeck, Germany

²DZHK (German Research Centre for Cardiovascular Research), Germany

³Max-Delbrück Center for Molecular Medicine, Berlin, Germany

⁴Charité-Universitätsmedizin Berlin, Charitéplatz 1, Berlin, Germany

⁵Institute of Experimental Hematology, Klinikum Rechts der Isar, Technische Universität München, Munich, Germany

*These authors contributed equally to the work.

Corresponding author:

Markus Schwaninger, Universität zu Lübeck Sektion Medizin, Ratzeburger Allee 160, Lübeck 23538, Germany.
Email: markus.schwanger@uni-luebeck.de

Loss of blood vessels is usually compensated by the formation of new ones, allowing for structural adaptation of the vasculature.⁶ However, in the healthy adult brain, ECs are quiescent and exhibit an extremely low turnover rate.⁷ Cerebral angiogenesis is only observed under pathological conditions, such as stroke. Here, angiogenesis is considered to promote tissue repair and functional recovery by supplying oxygen and nutrients for tissue regeneration, providing a scaffold for migration and directing neural progenitor cells towards the injured area.^{8–10} In contrast, angiogenesis plays a detrimental role in diabetic retinopathy and perhaps in Alzheimer's disease.^{9,10} It is still unclear whether angiogenesis also occurs in cerebral SVD and, if so, whether it affects the course of the disease.

We investigated the link between SVD and angiogenesis using a mouse model of the cerebral SVD incontinentia pigmenti (IP).¹¹ As a rare genetic disease caused by inactivating mutations in the X-chromosomal gene of the NF- κ B essential modulator (NEMO), IP affects skin, eyes, and the CNS.¹² CNS symptoms are related to the rarefaction of small vessels in all parts of the CNS.^{11,13,14} Hemizygous patients die during embryogenesis and only heterozygous female or, rarely, male mosaics survive. Neurological symptoms develop soon after birth and tend to improve thereafter.^{15,16} The cause of the recovery is still unknown.

In a mouse model of cerebral IP (*Nemo*^{beKO} mice), we found signs of endothelial proliferation. Angiogenesis, as indicated by vessel sprouting and intussusception, was closely linked to capillary rarefaction and hypoxic areas, but when new vessels formed, hypoxia regressed and mice recovered. With an ongoing injury, survival of newborn vessels was diminished, and mice developed signs of prolonged impairment. The present study demonstrates that angiogenesis can ensue in this model of cerebral SVD and may counteract functional deficits.

Material and methods

Animals

Brain endothelial-specific knockout (beKO) animals have been described previously.¹³ In general, all mouse lines were established on a C57BL/6 background. Brain endothelial-specific *Nemo* knockout (*Nemo*^{beKO}) animals were generated by crossing the BAC-transgenic *Slco1c1-CreER*^{T2} strain,¹⁷ which expresses the tamoxifen-inducible CreER^{T2} recombinase under control of the mouse *Slco1c1* regulatory sequences in brain ECs, with mice carrying loxP-flanked *Nemo* alleles (*Nemo*^{Fl}).¹⁸ Mice in which the constitutively active I κ B kinase 2 (IKK2, *IKK2ca*) was overexpressed in the brain were created by crossing *Slco1c1-CreER*^{T2} mice with *R26-Stop*^{FL}*Ikk2ca* (*Ikk2ca*^{StopFl/Fl}) mice.¹⁹ To enable

the assessment of recombination along the vascular tree, we generated *Slco1c1-Cre*^{GFP→HA} mice by crossing *Slco1c1-CreER*^{T2} and Tg(CAG-GFP,-Uprt)985Cdoe/Jx animals.²⁰ Due to the vascular specificity of the chicken actin CMV promoter,²¹ preferentially vascular cells in the brain of these mice express GFP until recombination. Recombined cells do not express GFP anymore but the HA-tagged UPRT. For bone marrow transplantation we used Actb-Egfp mice.²²

We treated transgenic mice with tamoxifen to induce Cre recombinase-mediated *Nemo* knockout, expression of *IKK2ca*, or expression of HA-tagged UPRT. In most experiments, mice received an intraperitoneal (i.p.) injection of 1 mg tamoxifen (Sigma-Aldrich, dissolved in 50 μ l of 90% miglyol 812 with 10% ethanol) per 20 g body weight every 12 h for five consecutive days. After tamoxifen injection, mice were referred to as *Nemo*^{beKO}, *Ikk2*^{beCA}, or *Slco1c1-Cre*^{GFP→HA}, respectively. In experiments investigating chronic *Nemo* deletion, we fed mice with chow containing 400 mg/kg tamoxifen citrate (265 mg/kg tamoxifen equivalent, Ssniff) for two to six weeks (14–43 days). In these experiments, animals were referred to as *Nemo*^{obeKO}. As the induction of CreER^{T2} in the *Slco1c1-CreER*^{T2} line has no effect by itself,¹⁷ we used littermates lacking the Cre transgene as controls in all experiments and referred to them as either *Nemo*^{Fl} or *Ikk2ca*^{StopFl/Fl} (in the tamoxifen injection-based experiments), or *Nemo*^{oFl} (in the oral tamoxifen-based experiments). Cre-negative control mice received the same tamoxifen treatment as the Cre-positive groups.

Mice were housed under a 12-h light/dark cycle and had access to food and water ad libitum. For all animal experiments, we used male and female littermate mice that were age- and gender-matched between experimental groups. All mice were 7–10 weeks of age at the beginning of experiments. The experimenter was blinded to the genotypes before the start of each experiment and during the analysis. All animal experiments complied with German laws and were approved by the local animal ethics committee (Ministerium für Landwirtschaft, Umwelt und ländliche Räume, Kiel, Germany). Experiments have been reported following the ARRIVE guidelines.

Brain ischemia

To induce ischemic strokes, we permanently occluded the distal middle cerebral artery (MCA) in male *Ikk2*^{beCA} mice and *Ikk2ca*^{StopFl/Fl} littermates 15 days after starting the tamoxifen injections. The procedure was described previously.²³ We anesthetized mice with tribromoethanol (15 μ l/g, 1.5% tribromoethanol, i.p.). A skin incision was made between ear and orbit on the left side and a burr hole was drilled to expose the stem

of the MCA after removing the muscle. The MCA was occluded (MCAO) by microbipolar electrocoagulation (Model ICC 50, Erbe). After the surgery, the skin incision was sutured, and the mice were placed under a heating lamp until they fully recovered. The surgery was performed under a microscope (Hund) and rectal temperature was maintained at 37°C with a heating pad. Mice were perfused 48 h after MCAO. Coronal cryosections (20 µm thick) were cut every 400 µm and infarct volumes were detected by using a silver staining technique.²⁴ Mortality was <10% and did not differ between the groups.

EdU administration

5-Ethynyl-2'-deoxyuridine (EdU, 25 µg/g body weight, Thermo Fisher Scientific) was injected i.p. twice on day 15 after starting the tamoxifen injections or as stated in the figure legends. The Click iT[®] EdU Alexa Fluor[®] 647 Imaging kit (Thermo Fisher Scientific) was used to detect the EdU signal.

In experiments using oral tamoxifen, mice received EdU in the drinking water (0.5 mg/ml) on days 11–14 of the tamoxifen diet and were either sacrificed on day 15 of the diet or changed back to normal drinking water and sacrificed on day 28 of the tamoxifen-containing diet.

Labeling of brain endothelial cells

To label brain ECs with GFP, the adeno-associated virus (AAV-BR1-CAG-eGFP) was injected intravenously (i.v.) into the lateral tail vein at a dose of 4×10^{11} genomic particles/mouse one week before starting the tamoxifen injections.²⁵ The GFP signal was detected by immunohistochemistry using anti-GFP antibodies (# ab13970, Abcam) and Alexa 488-labeled anti-chicken secondary antibodies (# ab150169, Abcam).

Biotin angiography

Mice were injected i.v. with sulfo-NHS-LC-biotin (EZ-Link; 5 mg/100 µl per mouse; Thermo Fisher Scientific) 1 h before perfusion. Biotin was detected on cryosections with Alexa Fluor 488-coupled streptavidin (# S11223, Invitrogen).

Hypoxia detection and white matter staining

A stock solution of the hypoxia probe (HP) was prepared by dissolving 100 mg pimonidazole HCl (Hypoxyprobe, Inc.) in 1 ml 0.9% NaCl. Mice received i.p. injections of a 1:10 diluted HP (60 µg/g body weight) 1 h before the perfusion. The probe was detected by immunostaining using rabbit anti-HP antibodies (# PAb2627AP, Hypoxyprobe Inc.). For white

matter staining, the HP staining was followed by a 20-min incubation with FluoroMyelin Green (Molecular Probes, Thermo Fisher Scientific, F34651, 1:300 in PBS) and by washing steps. Images of HP staining were taken before FluoroMyelin incubation.

In situ hybridization for *Nemo* mRNA

In situ hybridization (ISH) for *Nemo* mRNA was performed using the RNAscope[®] Multiplex Fluorescent Reagent Kit v2 (# 323110, Advanced Cell Diagnostics Inc., Hayward, CA, USA). Briefly, 20-µm thick cryosections were post-fixed at room temperature in 4% paraformaldehyde (PFA) for 15 min, dehydrated by ethanol, baked for 30 min at 37°C, and pretreated with hydrogen peroxide and protease IV. We incubated sections with double Z probes targeting mouse *Nemo* for 2 h at 40°C and hybridized sequentially with pre-amplifiers, amplifiers, and HRP-labeled oligonucleotides, followed by a TSA[®] Plus Cyanine 3 probe. After ISH, sections were subjected to the EdU click reaction and immunostaining of collagen IV (ColIV, # AB769, Millipore) and analyzed using a confocal microscope (SP5, Leica). Nuclei were counterstained with DAPI and sections were coverslipped with ProLong[™] Gold antifade reagent (Invitrogen). We controlled the RNA integrity of each sample with an RNAscope probe for RNA Polymerase II Subunit A (PolR2A) RNA (positive control) and nonspecific background with a probe for bacterial dihydrodipicolinate reductase (dapB) RNA (negative control). The *Nemo* probe consisted of a set of 20 double Z probes targeting the first six coding exons of *Nemo*, including the floxed exon 2 in *Nemo^{Fl}* animals (nucleotide 246-1135 of NM_001136067). Hybridization was identified as red punctuate dots or clusters.

Confocal images with 9-µm z-stacks were analyzed using Imaris 9.3.0 (Bitplane, Belfast, UK). Firstly, images were set in the “Display Adjustment” window to adjust the contrast value at the range (minimum to maximum) of 10–100 voxels for the EdU signal and 20–100 voxels for the *Nemo* signal. Vascular surfaces were created from ColIV immunostaining and smoothed under 0.5-µm surface details by using the “Surface” function in order to create the vessel mask to identify ECs. We then manually counted *Nemo*⁺ and EdU⁺ ECs in the masked images.

Immunohistochemistry

In most experiments, mice were perfused with 15–20 ml cold Ringer's solution supplemented with heparin (10 IU/ml). Brains were isolated, frozen and cut into 20-µm-thick sections using a cryostat at –20°C. Cryosections were fixed in methanol at –20°C, blocked

with 1% bovine serum albumin (BSA), and incubated overnight at 4°C with primary antibodies, followed by incubation with secondary antibodies for 1–2 h at room temperature.

ECs were stained with anti-CD31 antibodies (# 557355, BD-Pharmingen) and the basement membrane with anti-CollIV antibodies (# ab6586, Abcam; # AB769, Millipore or # 134001, Bio-Rad). EC nuclei were labeled with anti-ERG antibodies (# ab92513, Abcam), arterioles with anti-smooth muscle actin (SMA) antibodies (# DM001-05, Acris or # C6198-100UL, Millipore Sigma), hemagglutinin (HA) was stained with anti-HA antibodies (# sc-805, Santa Cruz), and neurons with anti-NeuN antibodies (# AB377, Millipore). To detect proliferating cells, we used anti-Ki67 antibodies (# ab16667, Abcam). Pericytes were labeled with anti-neuron-gial antigen 2 (NG2) antibodies (# AB5320, Millipore) in cryosections, whereas oligodendrocyte precursor cells (OPCs) were stained with the same antibodies in PFA-fixed free-floating sections.

Mice that received a bone marrow transplantation or viral vector administration were perfused with 15 ml cold Ringer's solution containing heparin (10 IU/ml), followed by 15 ml 4% cold PFA solution. Brains were post-fixed at 4°C for 2–4 h and stored at 4°C in the dark. Free-floating sections (50- to 100- μ m-thick) were blocked with 5% BSA in Tris-buffered saline containing 0.5% Triton for 1–2 h without further postfixation. GFP was detected with anti-GFP antibodies (# ab13970, Abcam). For staining of brain tissue of *Sleo1c1-Cre^{GFP→HA}* mice, free-floating sections (50 μ m) were blocked with 3% BSA in Tris-buffered saline containing 0.3% Triton for 6 h. Sections were incubated with primary antibodies at 4°C for 72 h and with secondary antibodies and DAPI at 4°C for 16 h. GFP was not amplified by antibodies.

Methods used for image analysis are described in the supplementary materials.

RNA isolation from cerebral vessel fragments

The cerebrum was isolated and dissected from the meninges. Brains were homogenized in DMEM/12 (Invitrogen) supplemented with 2 mM L-glutamine, 100 IU/ml penicillin, and 100 μ g/ml streptomycin, and the resulting homogenate was centrifuged at 1300g, 4°C, for 5 min. The pellet was suspended twice in 18% dextran solution (60,000–90,000 g/mol; Sigma-Aldrich) in PBS supplemented with 2 mM L-glutamine, 100 IU/ml penicillin, and 100 μ g/ml streptomycin and centrifuged at 6800g, 4°C, for 10 min to completely remove the supernatant and myelin debris. The pellet was washed in PBS and centrifuged at 1300g for 5 min. Then, the pellet was resuspended in PBS and filtered through a 70- μ m cell strainer. RNA was isolated from

vessel fragments retained on the cell strainer with the RNeasy[®] Mini kit (Qiagen) following the manufacturer's instructions.

RNA microarrays

The RNA was processed and hybridized on the Affymetrix Mouse Gene 2.0 Array (Thermo Fisher Scientific) as previously described.²⁶ RNA microarray results were analyzed with the Transcriptome Analysis Console 4.0 (TAC 4.0, Affymetrix, US). In total, 1094 transcripts were differentially regulated at least 2-fold with a pANOVA <0.05 and pFDR <0.05. Among these transcripts were 904 with valid gene symbols and Entrez IDs. Among these 904 transcripts, 896 corresponded to mouse genes. When analyzing the functional annotation of genes using the DAVID Bioinformatics Resource 6.8 (Leidos Biomedical Research, US) with the category UP_KEYWORDS, 742 transcripts clustered into 15 groups.

Quantitative RT-PCR

RNA (100 ng) from vessel fragments was transcribed with Moloney Murine Leukemia Virus Reverse transcriptase and random hexamer primers (Promega). Primers were designed to specifically target the floxed coding exon 2 of *Nemo*:¹⁸ forward, 5'-GGG AAC AGG CCT TAA AGG AG-3'; reverse, 5'-CTA AAG CTT GCC GAT CCT TG-3', product size 159 bp. *Actb* was used as a housekeeping gene: forward, 5'-ATG GAA TCC TGT GGC ATC CAT-3'; reverse, 5'-TTC TGC ATC CTG TCA GCA ATG-3', product size 140 bp.²⁷ Quantitative RT-PCR was performed according to the following protocol: 600 s at 95°C as preincubation, 3-step amplification (30 s at 95°C, 30 s at 60°C, and 30 s at 72°C for 40 cycles), and followed by melting (10 s at 95°C, 60 s at 65°C, and 1 s at 97°C). PCR products were amplified using the Platinum SYBR Green qPCR SuperMix (Invitrogen) and the LightCycler[®] 96 (Roche). Results were normalized to *Actb* using the $\Delta\Delta$ Ct method.

Behavioral tests

For voluntary wheel running, metal running wheels connected to bicycle tachometers (Sigma) were fit into mouse cages. Male mice were single-caged and had free access to the running wheels. The spontaneous locomotor activity was recorded daily. Mice were allowed to habituate to the setup for two weeks before the experiment. When the running speed of all mice reached a plateau, they received tamoxifen injections for five days as described above. Mice were kept in wheel-running cages until locomotor activity was recovered.

For the open-field test, mice were placed in an illuminated square arena (47 × 47 cm, 160 lux) and video-recorded for 10 min at the indicated time points after tamoxifen was injected. The inner zone was centered and defined as 25% of the overall area. We used the software ANY-maze (Stoelting Europe) to analyze the percentage of time spent in the inner zone which represents a parameter related to anxiety.

The object place recognition test (OPR test) was conducted as described previously.²⁸ Animals were handled for five days to adapt to the experimenter, followed by three consecutive days of habituation during which animals were placed into an empty open field (35 × 35 cm, 19 lux) for 10 min per day. One day after the last habituation day, the test consisted of a sample trial, followed by a 1-h retention interval, and a test trial. During the sample trial, two identical objects (glass bottles filled with sand of different colors, height 17–26 cm, bottom diameter 6–9 cm, heavy enough so that they could not be displaced by the mice) were positioned in two corners of the open field. Mice were put in the center of the open field and their explorative behavior towards the objects was video-recorded. The sample trial lasted 10 min. Mice were brought back to the home cage for a 1-h retention interval. In the test trial, two other objects, which were identical to the objects used in the sample trial, were positioned in the open field with one object displaced. While exploring the objects, mice were video-recorded for 5 min. Exploration of objects was quantified with the software ANY-maze (Stoelting Europe). A preference index for object exploration was calculated as the ratio of time exploring the displaced object and total exploration time. A preference index >0.5 indicates a preference for the displaced object, indicating the animals' memory for the position of the stationary objects.

Statistical analysis

All results are depicted as means ± SD. Two groups were compared by using an unpaired, two-tailed *t*-test. Welch's correction was used in the *t*-test when two groups did not have the same variance (significant *F* test for variance). When three or more groups were compared with one independent variable, a one-way analysis of variance (ANOVA) with Bonferroni's multiple comparison test was employed. For three or more groups with more than one independent variable, a two-way ANOVA with Bonferroni's post-test was used. To evaluate the correlation between Ki67⁺ ECs and active caspase 3⁺ ECs, a Pearson correlation test was applied. To analyze *Nemo*⁺ ECs in the ISH experiment, the ratios of *Nemo*⁺ ECs in the EdU⁺ and EdU⁻ were compared to the labeling efficiency of *Nemo*^{Fl}

mice (72.3%) by using a one-sample *t*-test. To analyze the preference index in the OPR test, the index was compared to the chance level 0.5 with a one-sample *t*-test. Values were considered significant at *P* values <0.05. All statistical analyses were performed with the GraphPad Prism software, version 5.0.

Results

Brain endothelial *Nemo* deletion induces endothelial cell proliferation

Similar to patients with IP, mice with an induced deficiency in *Nemo* in brain ECs (*Nemo*^{beKO}) partially recover at later time points.¹³ To search for underlying mechanisms, we profiled the cerebral vascular transcriptome of *Nemo*^{beKO} mice. When analyzing the functional annotation of genes that were differentially expressed at least 2-fold, we found that a cluster containing cell cycle/cell division/mitosis genes had the highest enrichment score of 19.6 among 15 clusters (Supplementary Table 1). Among 742 regulated genes, 77 genes (10.4%) were involved in cell cycle/cell division/mitosis (Figure 1(a), Supplementary Table 2). Out of these 77 genes, the expression of 75 genes was significantly higher in *Nemo*^{beKO} mice than in *Nemo*^{Fl} littermate controls (Figure 1(b)), suggesting an activation of cell mitosis in cerebral vessels of *Nemo*^{beKO} mice.

To test for active cell mitosis in the cerebral vessels, we sacrificed *Nemo*^{Fl} and *Nemo*^{beKO} mice at day 15 after the start of tamoxifen injection and stained brain sections for the proliferation marker Ki67 combined with the pan-endothelial marker CD31. The presence of Ki67⁺ cells along the vessels in the cortex (Figure 1(c)), hippocampus (Supplementary Figure 1), and other brain areas of *Nemo*^{beKO} mice, but not in the control mice, suggested that *Nemo* deletion in cerebral ECs induced robust proliferation in cerebral vessels.

To verify proliferation in brain microvessels, we injected EdU at day 10, day 12, and day 15 after beginning the tamoxifen injections. EdU was incorporated in the DNA of cells that were positive for ERG, a marker of endothelial nuclei, indicating that ECs proliferate (Figure 2(a)). EdU⁺ ECs occurred exclusively in the brain of *Nemo*^{beKO} mice, but not in *Nemo*^{Fl} controls (Figure 2(a) and (b)). Quantification revealed that 52.2% of EdU⁺ cells were endothelial (Figure 2(b) to (d)), and as many as 25.8% of ECs had incorporated EdU (Figure 2(e)). In addition to ECs, other cell types also proliferated (Figure 2(c) and (f)) some of which were localized in the vessel walls and represented pericytes (Figure 2(f); Supplementary Figure 2(a)). Using cell-specific markers for double staining, we identified other proliferating cells as oligodendrocyte precursor cells (OPCs) (Supplementary Figure 2(b)) and

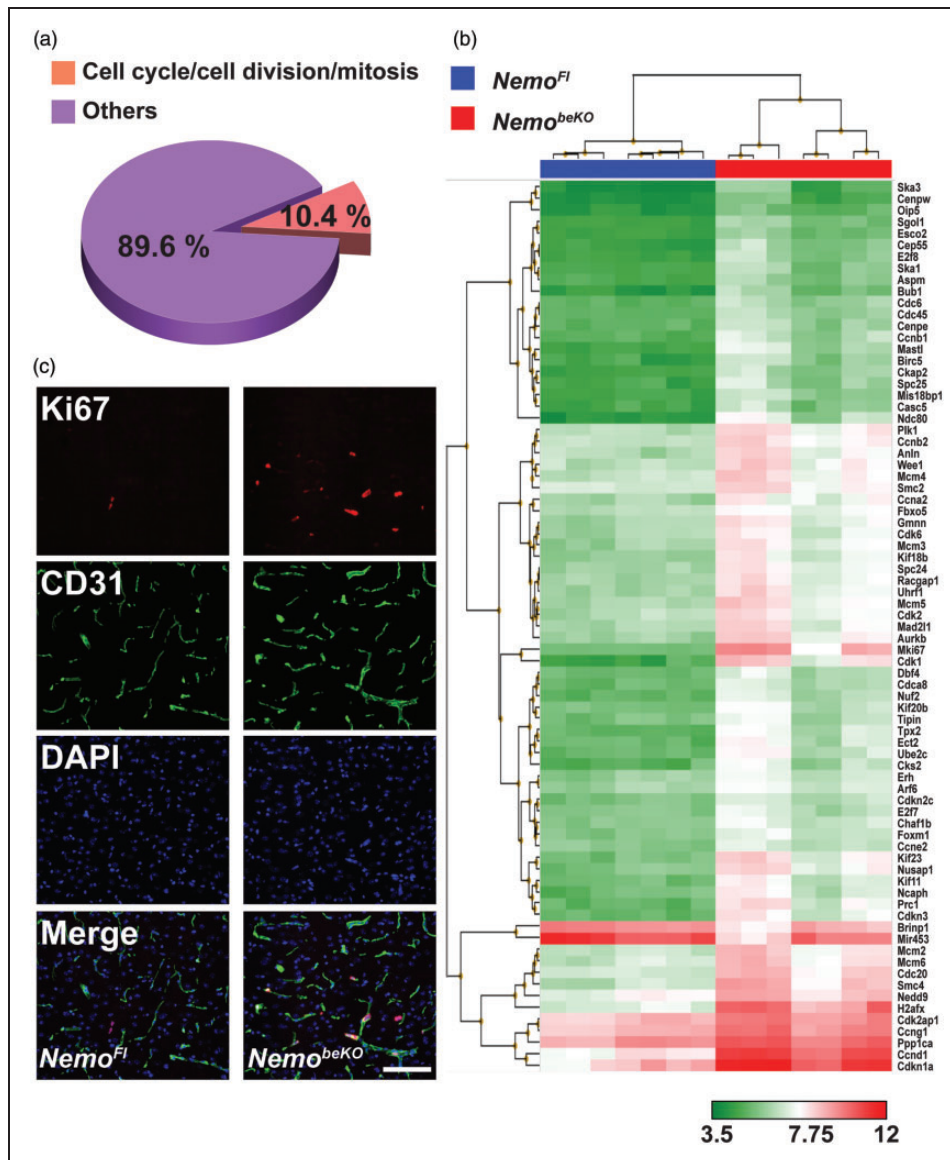


Figure 1. Inactivation of the *Nemo* gene induces cell mitosis in cerebral vessels. (a) Transcriptional profiling of cerebral vessels of *Nemo*^{beKO} mice and *Nemo*^{Fl} controls ($n = 7$) showed that, among the differentially expressed genes, 10.4% were involved in cell cycle/cell division/mitosis according to their functional annotations. The analysis included only transcripts with a change < -2 -fold or > 2 -fold and P -values (pANOVA and pFDR) < 0.05 . (b) Hierarchical clustering of the mitotic genes that were significantly changed in *Nemo*^{beKO} mice compared to control mice. (c) Representative immunostainings for Ki67 and CD31 showing proliferating cells along vessels in the cortex of *Nemo*^{beKO} but not *Nemo*^{Fl} mice, at day 15 after starting tamoxifen injections. Nuclei were stained with DAPI. Scale bar, 100 μm .

microglia (Supplementary Figure 2(c) and 2(d)). While most of our study focused on the cortex, angiogenesis was induced throughout the brain of *Nemo*^{beKO} mice, including cortex, corpus callosum, striatum, and hippocampus (Figure 2(g); Supplementary Figure 1(a)).

Brain endothelial *Nemo* deletion induces cerebral angiogenesis and vascular remodeling

With high-resolution confocal microscopy, we observed tip cells extending filopodia in the brain of

adult *Nemo*^{beKO} mice, indicating vessel sprouting (Figure 3(a); Supplementary Figure 3(a)). Such cells were not found in *Nemo*^{Fl} control brains. Some larger vessels with proliferating ECs seemed to split, providing evidence for vessel intussusception (Figure 3(b); Supplementary Video). Both morphological observations demonstrated cerebral angiogenesis and vascular remodeling in *Nemo*^{beKO} mice.

Formation of new vessels can involve proliferation of resident ECs or the recruitment of bone marrow-derived endothelial progenitor cells.^{8,29–31} To

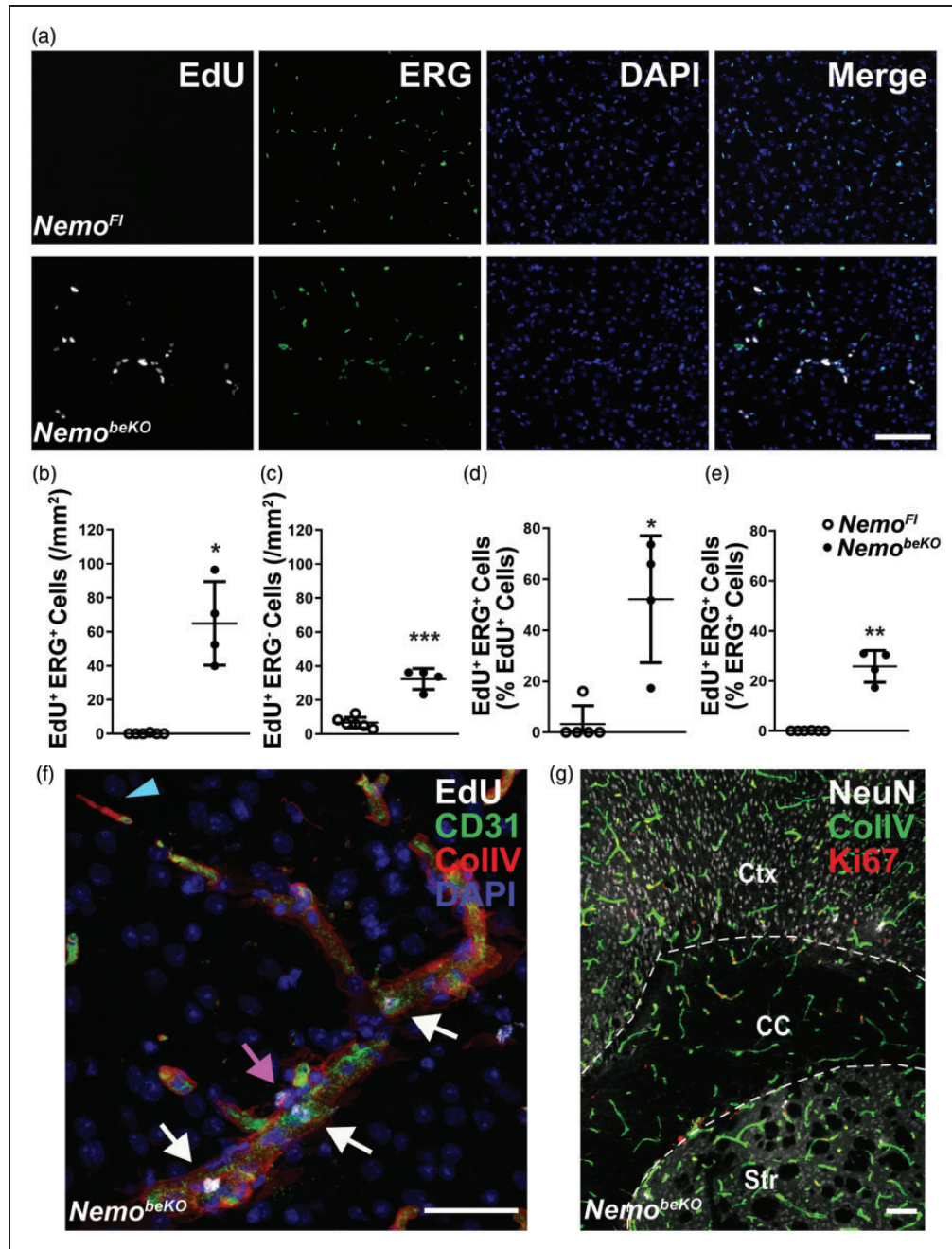


Figure 2. A large proportion of cerebral ECs in *Nemo^{beKO}* mice perform DNA synthesis. (a) Representative stainings for EdU and ERG revealed an increase in proliferation of ECs and non-ECs in the cortex of *Nemo^{beKO}* but not *Nemo^{Fl}* mice that received EdU at day 10, day 12, and day 15 and were killed on day 16 after starting tamoxifen injections. EdU incorporation is used as a marker of DNA synthesis and nuclei were stained with DAPI. Scale bar, 100 μm . (b)–(e) Quantification of proliferating ERG⁺ ECs (b), (d), (e) and ERG⁻ non-ECs (c) in the cortex of *Nemo^{beKO}* and *Nemo^{Fl}* mice ($n = 4-6$). The number of proliferating ECs (EdU⁺ERG⁺) is expressed as percentage of the total number of proliferating EdU⁺ cells (d) or as percentage of the total number of ERG⁺ ECs (e). Data are shown as means \pm SD, * $P < 0.05$, ** $P < 0.01$, *** $P < 0.001$, determined by two-tailed unpaired t -test with (b), (d) and (e), or without (c) Welch's correction. (f) Representative image stained for EdU, collagen IV (CollIV) and CD31, in high magnification showing a microvessel undergoing proliferation in the cortex of a *Nemo^{beKO}* mouse. Proliferating ECs (EdU⁺CD31⁺, white arrows) and non-ECs (EdU⁺CD31⁻, magenta arrow), and a string vessel (CollIV⁺CD31⁻ string-like structure, blue arrowhead) are shown in this image. Scale bar, 50 μm . (g) Representative staining for NeuN, CollIV and Ki67 showing proliferating cells along the vessels in different regions of the brain.

Ctx: cortex; CC: corpus callosum; Str: striatum.
Scale bar, 100 μm .

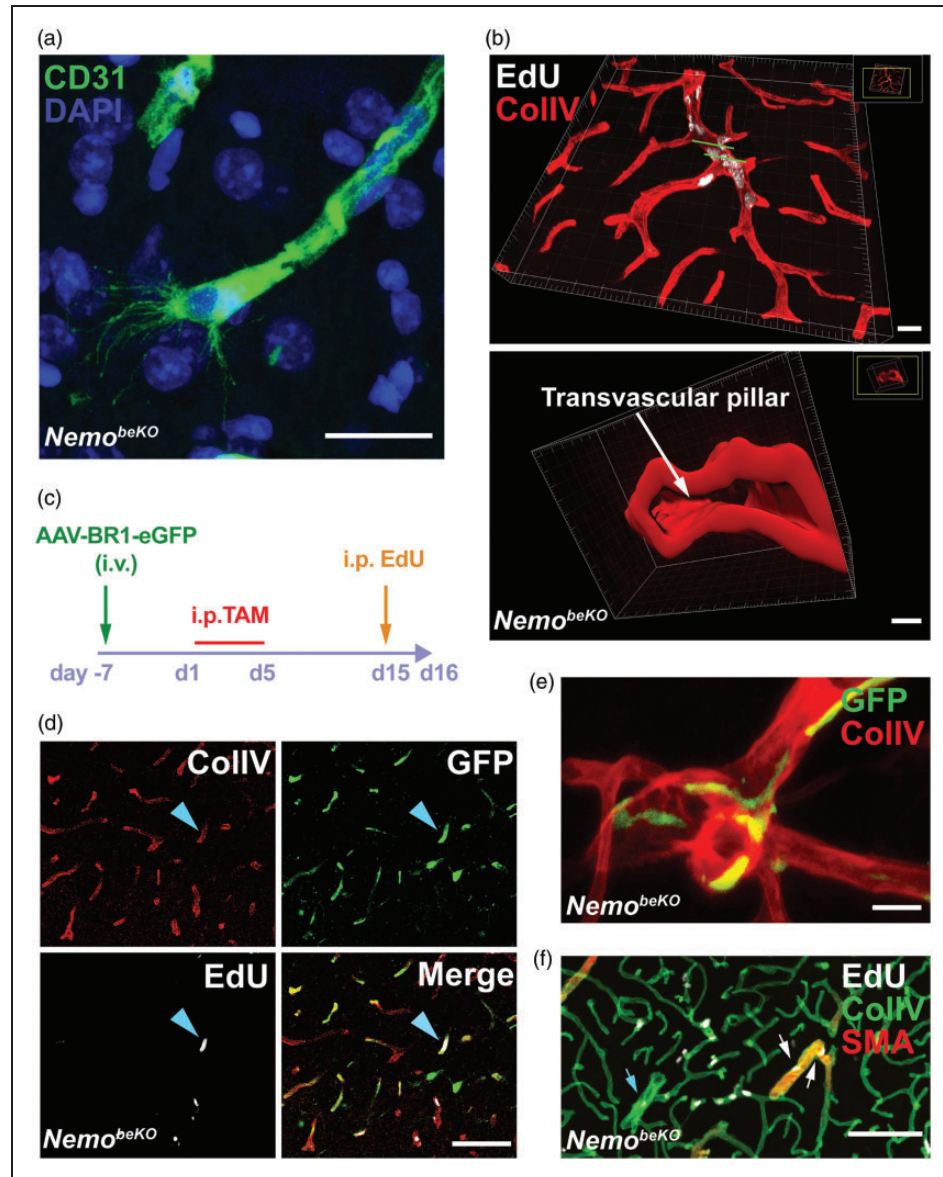


Figure 3. Angiogenesis in *Nemo*^{beKO} mice affects resident brain endothelial cells in all parts of the vascular tree. (a) Representative immunostaining for CD31 showing a tip cell with filopodia in the cortex of a *Nemo*^{beKO} mouse at day 16 after starting tamoxifen injections. Nuclei are stained by DAPI. Scale bars, 20 μm . (b) A 3D view of cortical vessels from a *Nemo*^{beKO} mouse stained for EdU and CollIV (top). In the bottom panel, a 3D cross-sectional view from the vessel fragment between two green lines in the top panel is presented, showing vessel intussusception. Scale bar, 20 μm (top) and 4 μm (bottom). (c) Scheme illustrating the workflow to label resident brain ECs with the AAV-BR1-eGFP virus before inducing *Nemo* deletion with tamoxifen and administering EdU. (d) Representative staining for CollIV, EdU and GFP from virus-injected mice showing proliferating resident ECs (EdU⁺GFP⁺, blue arrowhead). Scale bar, 100 μm . (e) Representative immunostaining for CollIV and GFP from bone marrow-transplanted *Nemo*^{beKO} mice, showing that bone marrow-derived cells were not ECs. Scale bar, 20 μm . (f) Representative staining for EdU, CollIV, and SMA at day 16 after starting tamoxifen injections, depicting proliferating EdU⁺ ECs in capillaries, SMA⁺ arterioles (white arrows) and venules (blue arrows). Scale bar, 100 μm .

investigate the origin of the proliferating ECs, we labeled resident brain ECs with GFP by injecting the vector AAV-BR1-eGFP, which selectively targets brain ECs,³² one week before starting the tamoxifen injections (Figure 3(c)). In *Nemo*^{beKO} mice, EdU-labeled ECs were positive for GFP, demonstrating that

proliferating cells originated from resident brain ECs (Figure 3(d)). To label bone marrow-derived cells, we transplanted *Actb-Egfp* bone marrow to *Nemo*^{beKO} mice. Two weeks after starting tamoxifen treatment, GFP⁺ cells had infiltrated the brains of *Nemo*^{beKO} mice and were mostly localized in close

proximity to blood vessels (Supplementary Figure 3(b), top), but they had the morphology of macrophages rather than ECs (Figure 3(e)), suggesting that they had differentiated into perivascular macrophages and were unlikely the source of proliferating ECs in the *Nemo^{beKO}* mice. In addition, some EGFP-labeled bone marrow-derived cells were found in the parenchyma in *Nemo^{beKO}* mice, but not in *Nemo^{Fl}* controls (Supplementary Figure 3(b)). Taken together, the data support the notion that resident ECs, not bone marrow-derived endothelial progenitor cells drive formation of new vessels in *Nemo^{beKO}* mice.

In contrast to the traditional concept that angiogenesis occurs only in venules and capillaries,³³ we observed endothelial proliferation in SMA⁺ arterioles as well as in capillaries and venules of *Nemo^{beKO}* mice (Figure 3(f)). This suggests that newborn endothelial cells replace the dead cells that we found in capillaries and bigger vessels of *Nemo^{beKO}* mice by using TUNEL and active caspase 3 staining (Supplementary Figure 3(c)).

Angiogenesis is associated with death of capillaries and hypoxia

Previous work has shown EC apoptosis, loss of capillaries, and the formation of string vessels in *Nemo^{beKO}* mice.¹³ The changes occurred in a time-dependent manner after inducing recombination with tamoxifen, raising the question as to whether vessel rarefaction and angiogenesis go hand in hand. To investigate this, we used cortex samples from our previous study in which we had sacrificed *Nemo^{beKO}* mice at six time points and had stained for active caspase 3 and CD31 as markers of EC death (Figure 2(b) in Ridder et al.¹³ and Supplementary Figure 3(c)). Double staining for Ki67 and CD31 showed that angiogenesis followed a time course (Figure 4(a)) similar to that for EC death (Figure 2(b) in Ridder et al.¹³). Indeed, EC proliferation correlated with EC death (Figure 4(b)), confirming the close temporal association.

To estimate the duration of EC proliferation, we administered EdU on day 15, when angiogenesis peaked, and quantified the rate of EdU⁺ cells expressing Ki67 on day 16 (1 day after EdU), day 22 (1 week after EdU), and day 45 (1 month after EdU, Figure 4(c)). On day 16, the majority of ECs that had synthesized DNA on day 15 were still positive for the mitosis marker Ki67 (Figure 4(d) and (e)). However, on day 22 only 7% of EdU⁺ cells remained in the cell cycle and on day 45 almost all cells had withdrawn from mitosis (Figure 4(e)), confirming the transient nature of angiogenesis.

Death of ECs leads to the formation of string vessels,⁵ many of which are present in the cortex and throughout the CNS of *Nemo^{beKO}* mice.¹³

Interestingly, endothelial cells often proliferated in close proximity to string vessels (Figures 2(f) and 4(f)). Therefore, to test whether angiogenesis is enhanced near string vessels, we stained sections of the cortex of *Nemo^{beKO}* mice for string vessels and Ki67⁺ ECs and segmented images into identical fields (155 × 155 μm²). Those fields containing string vessels were significantly more likely to contain Ki67⁺ ECs (Figure 4(f)) than fields without string vessels, suggesting a spatial association between vessel rarefaction and angiogenesis.

Vessel rarefaction led to a patchy hypoxia in the brains of *Nemo^{beKO}* mice as revealed by immunostaining for a hypoxia probe (Figure 4(g) and Supplementary Figures 4(c) and 5(d)). To test for a potential association between hypoxia and proliferation, we counted EdU⁺ vessels inside and outside of hypoxic zones that we defined as tissue within 150 μm of the nearest hypoxia probe staining (Supplementary Figure 4). The density of EdU⁺ vessels inside hypoxic zones was higher than outside, demonstrating that proliferation was occurring preferentially in hypoxic brain areas (Figure 4(g)).

Cerebral angiogenesis is a dynamic process leading to endothelial Nemo restoration and vascular repair

The above data suggest that hypoxia is a key stimulus of angiogenesis in this model of cerebral SVD. An additional factor to consider in the context of IP and *Nemo^{beKO}* mice is the deficiency of NF-κB signaling that has been reported to modulate angiogenesis; whether it enhances or inhibits angiogenesis, however, is still controversial.^{34–36} To assess the effect of NF-κB signaling on angiogenesis under hypoxic conditions, we induced focal cerebral ischemia by occluding the middle cerebral artery (MCAO) and used a mouse model that expresses a constitutively active mutant of *Ikk2* (*Ikk2ca*) in brain ECs (*Ikk2^{beCA}*).¹³ Expression of *Ikk2ca* in ECs activates NF-κB signaling without perturbing the microvasculature.¹³ Forty-eight hours after MCAO, infarct volumes did not differ between *Ikk2^{beCA}* mice and *Ikk2ca^{StopFl/Fl}* controls, suggesting a similar level of ischemia between the two genotypes (Figure 5(a)). Quantification of the total number of Ki67⁺ vessels in the contralateral nonischemic hemisphere showed a low level of proliferating vessels in *Ikk2^{beCA}* and control mice, whereas the number of Ki67⁺ vessels in the penumbra of the ischemic hemisphere was markedly increased and higher in *Ikk2^{beCA}* mice than in *Ikk2ca^{StopFl/Fl}* controls (Figure 5(b)), indicating that activation of NF-κB signaling is able to promote angiogenesis during hypoxia.

Due to the random inactivation of the heterozygous X-chromosomal *Nemo* mutation, IP patients typically display some degree of mosaicism between *Nemo*-competent and *Nemo*-deficient cells.³⁷ This corresponds to

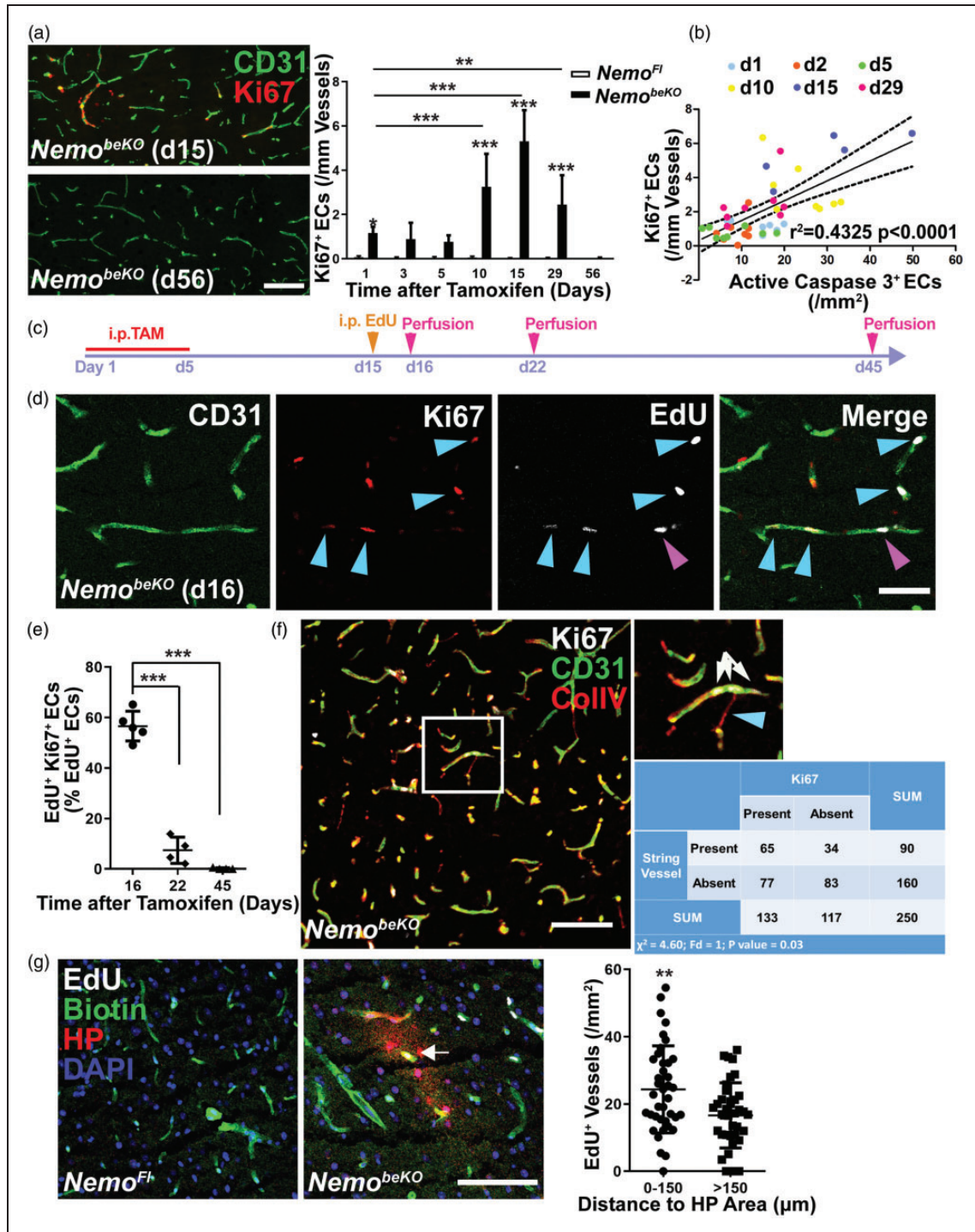


Figure 4. Angiogenesis is associated with vessel loss and hypoxia in *Nemo^{beKO}* mice. (a) Left panels, representative immunostainings for Ki67 and CD31 demonstrating angiogenesis in the cortex of *Nemo^{beKO}* mice at day 15 after starting tamoxifen injections (d15) but not at day 56 (d56). Right panel, quantification of Ki67⁺ cells in vessels of the cortex of *Nemo^{beKO}* and *Nemo^{Fl}* mice ($n = 5-8$) at seven time points after starting tamoxifen injections. Data are shown as means \pm SD, * $P < 0.05$, ** $P < 0.01$, *** $P < 0.001$, determined by two-way ANOVA with Bonferroni's post-test. Scale bar, 100 μ m. (b) Correlation between the number of Ki67⁺ ECs and active caspase 3⁺ ECs from *Nemo^{beKO}* mice at six time points, which are indicated by different colors ($n = 45$ mice). Values on the X-axis represent the numbers of active caspase 3⁺ cells in *Nemo^{beKO}* mice in a previous study,¹³ whereas the Y-axis shows the numbers of Ki67⁺ ECs from (a) that were quantified in sections from the same animals. Data are determined by Pearson correlation test. (c) Scheme illustrating the experimental strategy to determine Ki67 expression of EdU⁺ ECs. (d) Staining for EdU, Ki67, and CD31 revealed that EdU⁺ proliferating ECs in the cortex of *Nemo^{beKO}* mice differ in Ki67 expression at day 16 after starting tamoxifen

the genetic mosaicism in *Nemo*^{beKO} mice that is caused by incomplete recombination by CreER^{T2} although the *Slco1c1* locus that drives the CreER^{T2} expression is active in all segments of the CNS vasculature.^{13,38} We examined recombination along the vascular tree by crossing *Slco1c1-CreER^{T2}* mice with a line harboring the Cre-responsive double reporter allele CA-GFPstop-UPRT.²⁰ In the double transgenic *Slco1c1-Cre^{GFP→HA}* mice, endothelial cells express GFP prior to, and the HA-tagged UPRT, following Cre-mediated recombination. After injecting tamoxifen, we indeed observed capillaries and bigger vessels that had escaped recombination (Supplementary Figure 5(a)) supporting some degree of mosaicism. As a part of the remaining GFP signal in bigger vessels could originate from smooth muscle cells, we performed 3D reconstruction showing that the majority of cells in the inner endothelial layer of arterioles expressed HA-UPRT as a sign of recombination, whereas mural cells were GFP-positive (Supplementary Figure 5(b)). To investigate the effects of mosaic deletion in *Nemo*^{beKO} mice, we wanted to determine whether ECs with *Nemo* deletion (*Nemo*⁻) or those that escaped recombination (*Nemo*⁺) proliferate. To detect *Nemo* mRNA, we performed ISH using a probe that covers coding exons 1–6, including the exon 2 that is deleted in *Nemo*^{beKO} mice (Figure 5(c)). With this probe, 72.3% of ECs were *Nemo*⁺ in *Nemo^{Fl}* control mice, while only 59.7% ECs were *Nemo*⁺ in *Nemo*^{beKO} mice (Figure 5(d)). The rather high rate of *Nemo*⁺ cells in *Nemo*^{beKO} mice found by ISH contrasts to only 9.9% of residual *Nemo* mRNA determined by exon 2-specific quantitative RT-PCR (Figure 5(e)), indicating that the in situ probe also hybridized with the recombined *Nemo* mRNA to some degree. Despite the incomplete specificity of the *Nemo* ISH for the wild-type transcript, the rate of *Nemo*⁺ cells was significantly lower among EdU⁻ quiescent cells than among EdU⁺ proliferating cells in *Nemo*^{beKO} mice (Figure 5(f) and (g)), demonstrating that proliferation preferentially occurred in *Nemo*⁺ ECs. The notion that intact NF-κB signaling promotes angiogenesis also explains

why *Nemo* mRNA levels in vascular fragments of *Nemo*^{beKO} mice increased from day 14 to day 56, partially restoring endothelial *Nemo* expression in *Nemo*^{beKO} mice (Figure 5(e)).

Cerebral angiogenesis is associated with functional recovery

To label perfused vessels, we intravenously injected the reactive sulfo-NHS-LC-biotin. This technique demonstrated that newly formed vessels conducted blood (Figure 6(a)). Importantly, EdU⁺ ECs survived for at least 45 days after starting tamoxifen treatment (Figure 6(b)). Both findings suggest that proliferating ECs may restore vessel function. In accordance with this notion, quantification of the hypoxic area showed a decrease and later a complete disappearance of cerebral hypoxia in *Nemo*^{beKO} mice (Figure 6(c)).

To approach the question of whether angiogenesis is the basis for functional recovery in IP, we made use of the observation that *Nemo*⁺ ECs preferentially proliferate, rendering the newly formed cells particularly susceptible to Cre-mediated recombination in a prolonged tamoxifen treatment scheme. When continuously administering tamoxifen with the diet (*Nemo*^{obeKO} mice), we achieved a NEMO deficiency in ECs (reduction by 72.5%, Supplementary Figure 6(a)) similar to that in *Nemo*^{beKO} animals. *Nemo*^{obeKO} mice developed pathological disorders, including increased IgG extravasation (Supplementary Figure 6(b) and (c)), EC apoptosis (Supplementary Figure 6(d)), and string vessels (Supplementary Figure 6(e) and (f)), as in the *Nemo*^{beKO} mice,¹³ suggesting that the oral route can substitute for i.p. injection of tamoxifen. Prolonging oral treatment up to 41 days led to a persistently high level of endothelial proliferation (Figure 6(d)). However, survival of newly formed EdU⁺ ECs was compromised (Figure 6(e)) in contrast to what we had observed with transient i.p. administration of tamoxifen (Figure 6(b)). Consequently, the hypoxic area continued to increase on tamoxifen diet (Figure

Figure 4. Continued.

injections. Some ECs that had incorporated EdU stopped proliferating (EdU⁺Ki67⁻, magenta arrowhead), others were still in mitosis (EdU⁺Ki67⁺, blue arrowheads). Scale bar, 50 μm. (e) Quantification of EdU⁺Ki67⁺ ECs in the cortex of *Nemo*^{beKO} mice (*n* = 4–5) at three time points after the start of tamoxifen injection demonstrated a gradual decrease in the number of the EdU⁺ ECs that sustained proliferation. Data are shown as means ± SD, ****P* < 0.001, determined by one-way ANOVA with Bonferroni's post-tests. (f) Immunostaining in the cortex of a *Nemo*^{beKO} mice showing that proliferating ECs (Ki67⁺CD31⁺) and string vessels (CollIV⁺CD31⁻ string-like structures) were spatially associated. A representative image is shown, with a high magnification view of the white-framed region as inset. Blue arrowhead, string vessel; white arrows, vessel with proliferating ECs. In the analysis, 10 fields from 5 *Nemo*^{beKO} mice were analyzed. Scale bar, 100 μm. (g) Staining for biotin, hypoxia probe (HP), and EdU demonstrated proliferating vessels inside of hypoxic areas (white arrow) in the cortex of *Nemo*^{beKO} and not in *Nemo^{Fl}* mice. Mice received an i.v. injection of sulfo-NHS-LC-biotin for vessel labeling. Nuclei were stained with DAPI. Quantification of proliferating vessels inside and outside of hypoxic areas (defined as regions within 150 μm of HP⁺ staining). Data are means ± SD (39 fields from 5 *Nemo*^{beKO} mice). ***P* < 0.01, determined by two-tailed unpaired t-test. Scale bar, 100 μm.

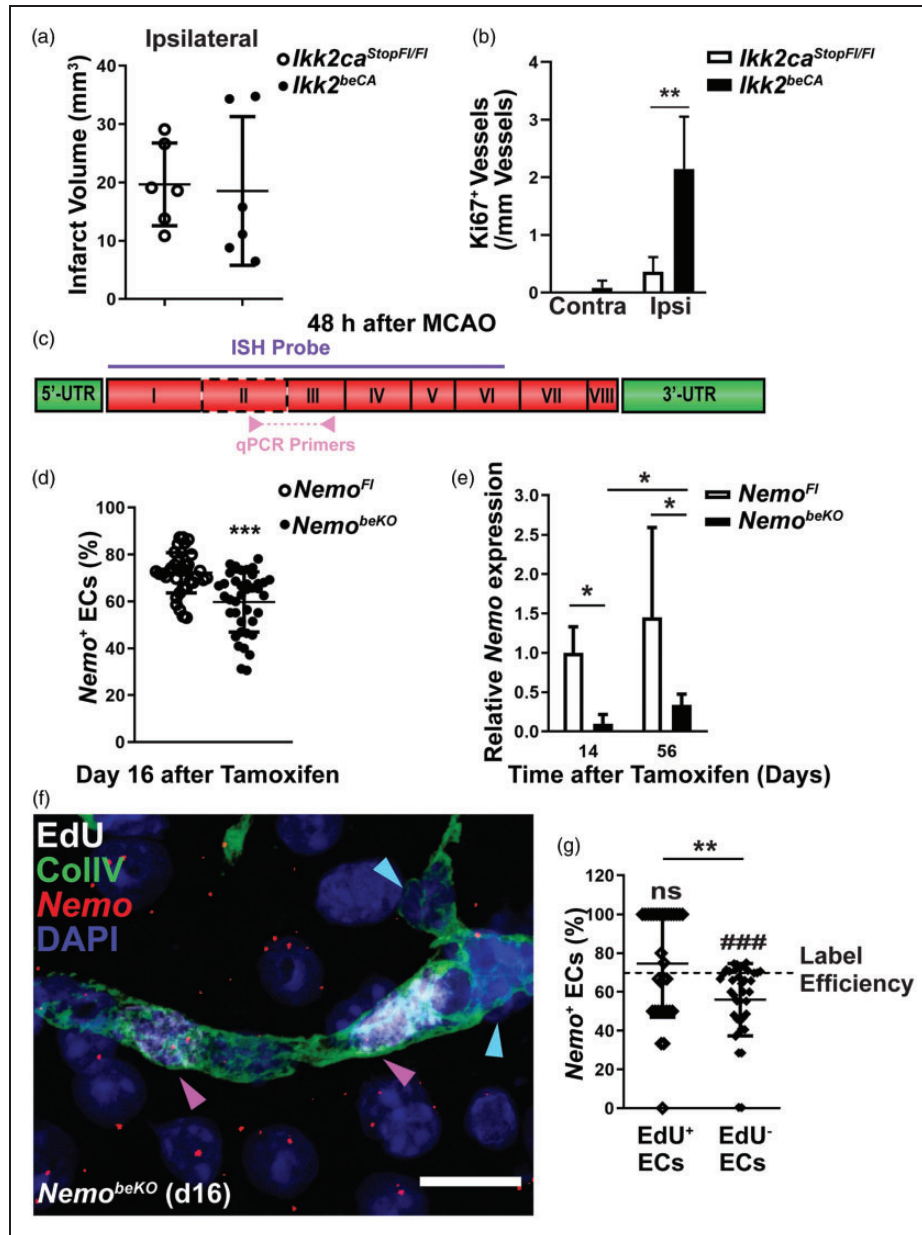


Figure 5. NF- κ B signaling promotes endothelial proliferation in cerebral ischemia. (a) Constitutive activation of IKK2 in the brain endothelium ($Ikk2^{beCA}$) did not affect infarct sizes at 48 h after MCAO in comparison to $Ikk2ca^{StopFI/FI}$ controls ($n = 6$). Data are shown as means \pm SD, determined by two-tailed unpaired t -test. (b) Quantification of Ki67 $^{+}$ vessels in the contralateral hemisphere (Contra) and penumbral area of ipsilateral hemisphere (Ipsi) revealed that the constitutive activation of IKK2 enhanced angiogenesis at 48 h in the ipsilateral but not in the contralateral hemisphere after MCAO ($n = 6$ mice). Data are shown as means \pm SD, $^{**}P < 0.01$, determined by two-way ANOVA with Bonferroni's post-test. (c) A diagram of the *Nemo* mRNA transcript with eight coding exons created according to NM_001136067. The regions targeted by ISH probes and qPCR primers are indicated. Coding exon 2 (framed by dashed line) is flanked by loxP sites in *Nemo^{FI}* mice.¹⁸ (d) Quantification of *Nemo⁺* ECs presented as a percentage of total ECs in ISH of *Nemo^{beKO}* and control cortex demonstrated a reduction of *Nemo⁺* ECs in *Nemo^{beKO}* mice (38–39 fields from two animals of each group). Data are shown as means \pm SD, $^{***}P < 0.001$, determined by two-tailed unpaired t -test with Welch's correction. (e) Expression levels of *Nemo* mRNA that were determined by real-time qPCR in vessel fragments of *Nemo^{beKO}* mice and *Nemo^{FI}* controls ($n = 4$ –5) at day 14 and 56 indicated a partial restoration of *Nemo* expression in *Nemo^{beKO}* mice. Data are shown as means \pm SD, $^{*}P < 0.05$ determined by two-way ANOVA with Bonferroni's post-test. (f) Representative image of fluorescent ISH for *Nemo* mRNA combined with EdU and ColIV staining showing a vessel composed of *Nemo⁺* and *Nemo⁻* ECs. *Nemo⁺* ECs (magenta arrowheads) had incorporated EdU $^{+}$, while *Nemo⁻* ECs (blue arrowheads) were EdU $^{-}$ in the same vessel. Scale bar, 20 μ m. (g) The fraction of *Nemo⁺* ECs was significantly lower among EdU $^{-}$ ECs compared to EdU $^{+}$ ECs (39 fields from two *Nemo^{beKO}* mice were analyzed). The numbers of *Nemo⁺* ECs in EdU $^{+}$ and EdU $^{-}$ ECs were compared to the labeling efficiency of *Nemo* ISH in *Nemo^{FI}* mice from Figure 5(d) (72.3%). Data are shown as means \pm SD, $^{**}P < 0.01$, $^{###}P < 0.001$, determined by two-tailed unpaired t -test with Welch's correction and one sample t -test.

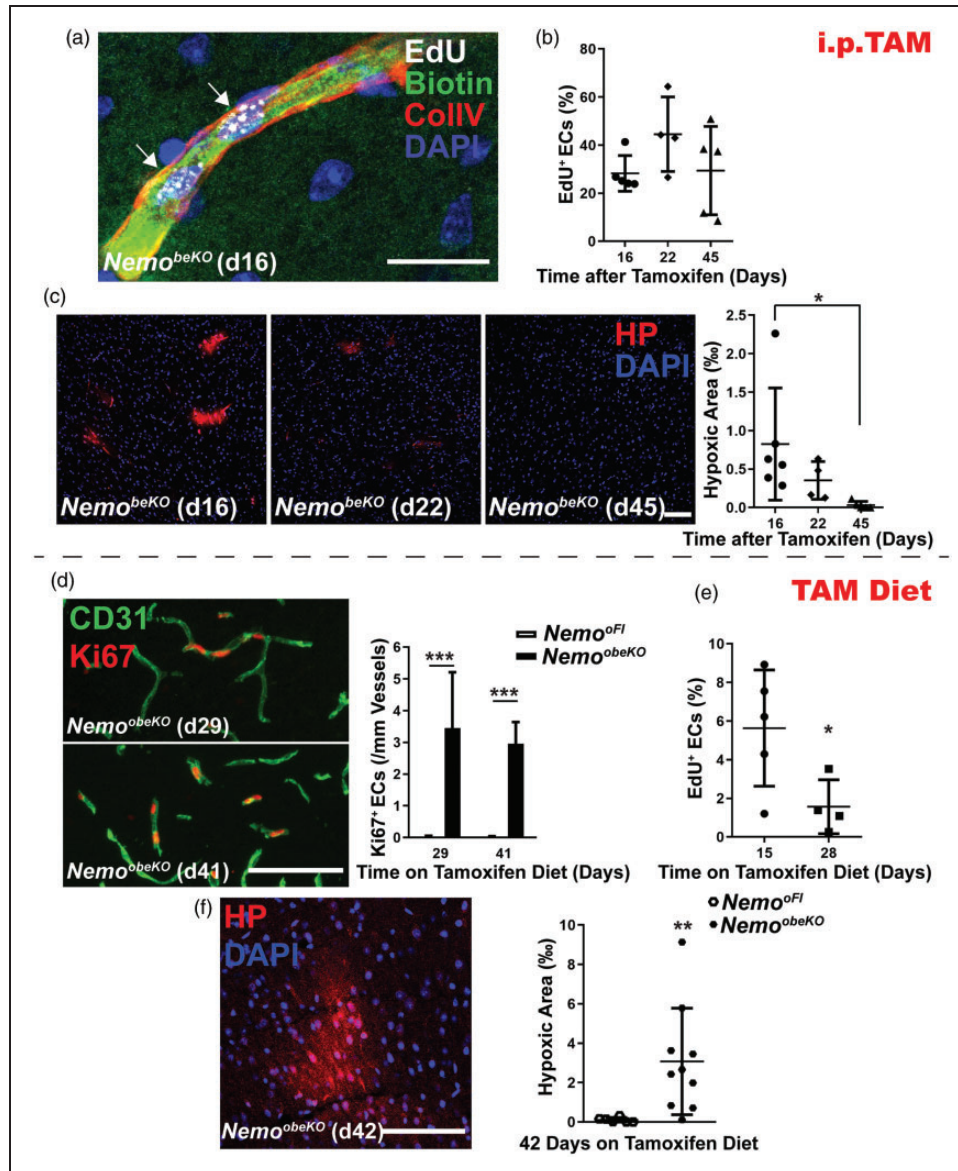


Figure 6. Ongoing *Nemo* ablation interferes with effective angiogenesis. (a) Stainings for EdU, biotin, and CollIV of the cortex after *Nemo^{beKO}* mice received an i.v. injection of sulfo-NHS-LC-biotin to label perfused vessels. A representative image demonstrates a perfused vessel composed of two daughter ECs (white arrows). Nuclei were stained with DAPI. Scale bar, 50 μ m. (b) The number of EdU⁺ proliferating ECs in the cortex of *Nemo^{beKO}* mice ($n = 5-6$) remained stable up to 45 days after starting tamoxifen injections. The experimental design is depicted in Figure 4(c). Numbers of EdU⁺ ECs are presented as percentage of total ECs. Data are shown as means \pm SD, determined by one-way ANOVA with Bonferroni's multiple comparison test. (c) Left panel, representative staining for hypoxia probe (HP) and nuclei (DAPI) in the cortex of *Nemo^{beKO}* mice at three time points after starting tamoxifen injections. Right panel, quantification of the hypoxic areas in the cortex of *Nemo^{beKO}* mice ($n = 4-6$). Hypoxic areas are presented as per mill of the investigated cortical area. Data are shown as means \pm SD, * $P < 0.05$, determined by one-way ANOVA with Bonferroni's multiple comparison test. Scale bar, 100 μ m. (d) When mice were fed a tamoxifen diet to maintain ongoing *Nemo* ablation (*Nemo^{obeKO}*), immunostainings for Ki67 and CD31 showed persistent angiogenesis. Left panel, representative images. Right panel, quantification of proliferating ECs in both *Nemo^{obeKO}* mice and control mice ($n = 7-8$). Data are shown as means \pm SD, *** $P < 0.001$, determined by two-way ANOVA with Bonferroni's post-test. Scale bar, 100 μ m. (e) The number of EdU⁺ newborn ECs in the cortex dropped over time when *Nemo^{obeKO}* mice ($n = 4-5$) were fed a tamoxifen containing diet. Mice were treated with EdU in the drinking water on days 11-14 of the tamoxifen diet. Cell numbers are presented as percentage of total ECs. Data are shown as means \pm SD, * $P < 0.05$, determined by two-tailed unpaired t-test. (f) Left panel, representative immunostaining for hypoxia probe (HP) and CD31 showing a hypoxic area in the cortex of a *Nemo^{obeKO}* mouse 42 days on tamoxifen diet. Right panel, quantification of hypoxic areas showed a significant increase in *Nemo^{obeKO}* mice in comparison to control mice ($n = 7-10$) after 42 days of tamoxifen diet. Hypoxic areas are presented as per mill of the investigated cortical area. Data are shown as means \pm SD, ** $P < 0.01$, determined by two-tailed unpaired t-test with Welch's correction. Scale bar, 100 μ m.

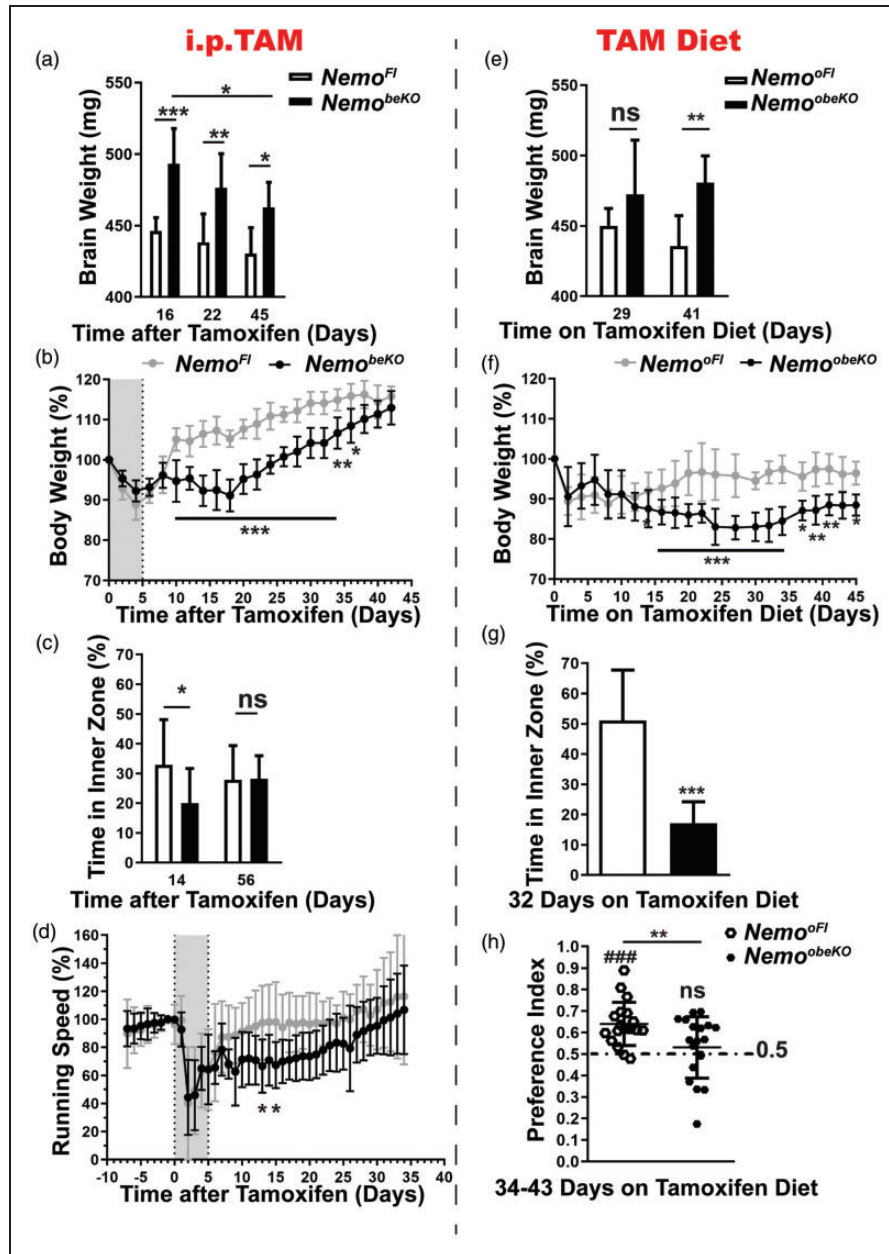


Figure 7. Angiogenesis ameliorates pathological outcomes in *Nemo^{beKO}* mice. (a) Brain weight (without olfactory bulbs) of *Nemo^{beKO}* and *Nemo^{Fl}* mice ($n = 5-9$) at three time points after the start of tamoxifen injection indicated a moderate reduction of brain edema. Data are shown as means \pm SD, $*P < 0.05$, $**P < 0.01$, $***P < 0.001$, determined by two-way ANOVA with Bonferroni's post-test. (b) The body weight of *Nemo^{beKO}* mice dropped after starting tamoxifen injections (indicated as grey field), but recovered until day 45. Values are presented as a percentage of the body weight at day 0 ($n = 5-7$ mice per genotype). Data are shown as means \pm SD, $*P < 0.05$, $**P < 0.01$, $***P < 0.001$, determined by two-way ANOVA with Bonferroni's post-test. (c) On day 14 after starting tamoxifen injections, *Nemo^{beKO}* mice spent less time in the inner zone of the open field than *Nemo^{Fl}* controls indicating anxiety-like behavior but the parameter did not significantly differ at day 56 ($n = 8-12$ mice per genotype). Data are shown as means \pm SD, $*P < 0.05$, determined by two-way ANOVA with Bonferroni's post-test. (d) *Nemo^{beKO}* mice showed a lower locomotor activity in running wheels after tamoxifen injection (grey field) in comparison to *Nemo^{Fl}* controls ($n = 11-13$). However, the activity normalized until day 30. Running speed is expressed as percentage of the mean speed on days -1 and 0 . Data are shown as means \pm SD, $*P < 0.05$, determined by two-way ANOVA with Bonferroni's post-test. (e) The brain weight (without olfactory bulbs) of *Nemo^{beKO}* mice remained stable at an increased level in comparison to *Nemo^{Fl}* controls up to day 41 after starting the tamoxifen diet ($n = 7-8$ mice per genotype). Data are shown as means \pm SD, $*P < 0.01$, determined by two-way ANOVA with Bonferroni's post-test. (f) The body weight of *Nemo^{beKO}* mice dropped during oral tamoxifen treatment and remained at a lower level in comparison to *Nemo^{Fl}* mice up to day 45. Values are presented as percentage of body weight at day 0 ($n = 7-22$ mice per genotype). Data are shown as means \pm SD,

6(f)) and did not decrease as after transient i.p. administration of the drug (Figure 6(c)).

Interestingly, productive angiogenesis that followed the transient tamoxifen administration was associated with recovery of several functional parameters. We observed a decrease in brain weights of *Nemo^{beKO}* mice as a sensitive marker for brain edema over time (Figure 7(a)). In addition, body weights of *Nemo^{beKO}* mice gradually increased to the level of control mice (Figure 7(b)). As reported previously,¹³ *Nemo^{beKO}* mice transiently showed anxiety-like behavior in the open field but this normalized at later time points (Figure 7(c)). Finally, voluntary wheel running was reduced for about 25 days but improved at later time points (Figure 7(d)).

In contrast, recovery was impaired in *Nemo^{obeKO}* mice with futile angiogenesis. Brain weights remained at a similar level (Figure 7(e)) and body weights only slowly improved after day 35 (Figure 7(f)). In parallel, *Nemo^{obeKO}* mice still showed marked anxiety-like behavior at day 32 (Figure 7(g)). Although we found no obvious changes in the white matter structure (Supplementary Figure 5(c)), we consistently observed hypoxic areas in the corpus callosum of *Nemo^{beKO}* mice as a characteristic feature of small vessel diseases (Supplementary Figure 5(d)). In line with this notion, *Nemo^{obeKO}* mice performed poorly in the object place recognition task in comparison to *Nemo^{oFl}* controls that could distinguish the displaced objects, suggesting memory deficits of the long-term *Nemo*-deficient mice (Figure 7(h)). This feature makes *Nemo^{obeKO}* mice a suitable model to study behavioral consequences of SVD.

Discussion

Loss of microvessels represents a pivotal step in the pathogenesis of SVD but angiogenesis may potentially compensate for the vessel rarefaction. Still, surprisingly little is known about vessel remodeling and endothelial proliferation in SVD. We have investigated the role of angiogenesis in IP, a genetic disease that leads to cerebral SVD. Our data provide evidence for a profound remodeling of the microvasculature following disease onset. In contrast to the healthy adult brain, in which the endothelium is highly quiescent, at least one-fourth of ECs underwent proliferation in the cortex.

Angiogenesis seemed to involve all types of small vessels, including arterioles, capillaries, and venules, and occurred in the form of sprouting and intussusception. Vessel rarefaction seems evenly distributed across CNS regions but resident ECs preferentially proliferated near string vessels. Whether sprouting vessels use the empty basement membrane string as a guide structure is still unclear. The spatial association of endothelial proliferation with hypoxic areas suggests that hypoxia or ischemia in SVD brains are important stimuli for angiogenesis.¹ Hypoxia or blood-derived molecules that reach the brain parenchyma due to the blood–brain barrier damage may stimulate the proliferation of non-endothelial cells in the brain of *Nemo^{beKO}* mice.^{39–42}

In addition to hypoxia, inhibition of NF- κ B signaling, which occurs in a mosaic pattern in IP and *Nemo^{beKO}* mice, may affect angiogenesis. Although NF- κ B activity favors proliferation,³⁶ there is evidence in the literature that endothelial NF- κ B may inhibit angiogenesis.^{34,35} In apparent agreement with this concept, we found an induction of angiogenesis when we inhibited NF- κ B signaling in endothelial cells. However, on closer inspection it turned out that proliferating ECs were more often *Nemo*-competent than quiescent ECs. Moreover, angiogenesis increased, when we activated NF- κ B in the context of focal cerebral ischemia. Both findings indicate that, in tissues with cellular heterogeneity and mosaicism, NEMO-deficient ECs may send an angiogenic signal to NEMO-competent ECs that subsequently proliferate, at least in cerebral ischemia and IP. In these disorders, ECs die suggesting as an alternative explanation that NF- κ B enhances angiogenesis simply by supporting endothelial survival.^{13,38} Both the preferential death of *Nemo⁻* and the predominant angiogenesis of *Nemo⁺* ECs are expected to increase the ratio of cells with intact *Nemo* gene, in keeping with what we have observed (Figure 5(e)). Over time, this results in a partial genetic rescue, a phenomenon that is known as skewing in IP and other X-chromosomal diseases.³⁷

Skewing may explain why angiogenesis is successful in IP and *Nemo^{beKO}* mice and why it is associated with functional recovery. The monophasic course of neurological symptoms clearly sets IP apart from other models of cerebral SVDs. In typical SVDs,

Figure 7. Continued.

* $P < 0.05$, ** $P < 0.01$, *** $P < 0.001$, determined by two-way ANOVA with Bonferroni's post-test. (g) On day 32 after starting the tamoxifen diet, *Nemo^{obeKO}* mice spent less time in the inner zone of the open field, indicating increased anxiety-like behavior in comparison to *Nemo^{oFl}* mice ($n = 12$). Data are shown as means \pm SD, *** $P < 0.001$, determined by two-tailed unpaired t -test with Welch's correction. (h) In the object place recognition test, *Nemo^{obeKO}* mice fed for 34–43 days with tamoxifen diet showed no preference for the displaced object and performed worse than *Nemo^{oFl}*. The statistical results of the test between the preference index and the chance level (0.5, dashed line) are shown above the related column ($n = 19$ mice per genotype). Data are shown as means \pm SD. ** $P < 0.01$, ### $P < 0.001$, determined by two-tailed unpaired t -test and one sample t -test.

neurological symptoms progress, probably because noxious stimuli persist and interfere with angiogenesis. When we modeled the ongoing presence of a noxious stimulus by continuously administering tamoxifen in the diet, newborn ECs did not survive and hypoxic areas increased over time. Unsuccessful angiogenesis was associated with prolonged functional impairment and the additional development of memory deficits. This avenue may lead to severe cognitive impairment in SVD. However, the observation of angiogenesis in a model of SVD gives hope that, if angiogenesis is effective, the progression of the disease can be stopped. To achieve this goal, it will be important to understand the limitations of productive angiogenesis in SVD. One important cause is the old age of patients with typical SVD in contrast to the young IP patients. Angiogenesis decreases with age but the mechanisms underlying this decrease are still unknown.⁷ In addition to age, other disease-specific factors may prevent successful angiogenesis in SVDs. Understanding the regulation and overcoming possible restrictions of cerebral angiogenesis may help to improve the therapy of IP and adult forms of SVD.

Acknowledgements

We thank Beate Lembrich, Frauke Spiecker, and Ines Stölting, Lübeck, Germany for expert technical assistance.

Authors' contributions

YJ, JW and MS conceived, designed, and planned the main concept of the work. YJ, JL and JW performed the angiogenesis experiments. YJ, KM investigated the time course. JW and JCA designed and conducted the bone marrow transplantation. MK performed AAV experiments. DAR and MAK performed experiments on cerebral ischemia. MR and KK investigated the distribution of recombination. NH performed microarray analyses. MSS provided valuable tools and support for drafting the manuscript. YJ and MS conceptualized and interpreted the data and drafted the manuscript.

Funding

The author(s) disclosed receipt of the following financial support for the research, authorship, and/or publication of this article: This study was supported by grants of the Deutsche Forschungsgemeinschaft (SCHW 416/5-2, 5-3, GRK 1957), the European Union's Seventh Framework Programme FP7 under grant agreement 607962 (nEUROinflammation), and the European Research Council (ERC) under the European Union's Horizon 2020 research and innovation programme (grant agreement No 810331) to MS. We are grateful for the kind support of Incontinentia Pigmenti France.

Declaration of conflicting interests

The author(s) declared no potential conflicts of interest with respect to the research, authorship, and/or publication of this article.

ORCID iDs

Mahtab A. Khan  <https://orcid.org/0000-0001-5703-2730>
Jan Wenzel  <https://orcid.org/0000-0001-6313-2439>
Markus Schwaninger  <https://orcid.org/0000-0002-4510-9718>

Supplemental material

Supplemental material for this article is available online.

References

- Pantoni L. Cerebral small vessel disease: from pathogenesis and clinical characteristics to therapeutic challenges. *Lancet Neurol* 2010; 9: 689–701.
- van Leijsen EM, Bergkamp MI, van Uden IW, et al. Cognitive consequences of regression of cerebral small vessel disease. *Eur Stroke J* 2019; 4: 85–89.
- Kalaria RN. Cerebrovascular disease and mechanisms of cognitive impairment: evidence from clinicopathological studies in humans. *Stroke* 2012; 43: 2526–2534.
- Brown WR, Blair RM, Moody DM, et al. Capillary loss precedes the cognitive impairment induced by fractionated whole-brain irradiation: a potential rat model of vascular dementia. *J Neurol Sci* 2007; 257: 67–71.
- Brown WR, Moody DM, Thore CR, et al. Microvascular changes in the white matter in dementia. *J Neurol Sci* 2009; 283: 28–31.
- Pries AR and Secomb TW. Making microvascular networks work: angiogenesis, remodeling, and pruning. *Physiology* 2014; 29: 446–455.
- Harb R, Whiteus C, Freitas C, et al. In vivo imaging of cerebral microvascular plasticity from birth to death. *J Cereb Blood Flow Metab* 2013; 33: 146–156.
- Beck H and Plate KH. Angiogenesis after cerebral ischemia. *Acta Neuropathol* 2009; 117: 481–496.
- Kojima T, Hirota Y, Ema M, et al. Subventricular zone-derived neural progenitor cells migrate along a blood vessel scaffold toward the post-stroke striatum. *Stem Cells* 2010; 28: 545–554.
- Thored P, Wood J, Arvidsson A, et al. Long-term neuroblast migration along blood vessels in an area with transient angiogenesis and increased vascularization after stroke. *Stroke* 2007; 38: 3032–3039.
- Müller K, Courtois G, Ursini MV, et al. New insight into the pathogenesis of cerebral small-vessel diseases. *Stroke* 2017; 48: 520–527.
- Bodemer C. Incontinentia pigmenti and hypomelanosis of Ito. *Handbook Clin Neurol* 2013; 111: 341–347.
- Ridder DA, Wenzel J, Müller K, et al. Brain endothelial TAK1 and NEMO safeguard the neurovascular unit. *J Exp Med* 2015; 212: 1529–1549.

14. Goldberg MFMD. The skin is not the predominant problem in incontinentia pigmenti. *Arch Dermatol* 2004; 140: 748–750.
15. Minic S, Trpinac D and Obradovic M. Systematic review of central nervous system anomalies in incontinentia pigmenti. *Orphanet J Rare Dis* 2013; 8: 25.
16. Meuwissen ME and Mancini GM. Neurological findings in incontinentia pigmenti: a review. *Eur J Med Genet* 2012; 55: 323–331.
17. Ridder DA, Lang MF, Salinin S, et al. TAK1 in brain endothelial cells mediates fever and lethargy. *J Exp Med* 2011; 208: 2615–2623.
18. Schmidt-Suppran M, Bloch W, Courtois G, et al. NEMO/IKK gamma-deficient mice model incontinentia pigmenti. *Mol Cell* 2000; 5: 981–992.
19. Sasaki Y, Derudder E, Hobeika E, et al. Canonical NF-kappaB activity, dispensable for B cell development, replaces BAFF-receptor signals and promotes B cell proliferation upon activation. *Immunity* 2006; 24: 729–739.
20. Gay L, Miller MR, Ventura PB, et al. Mouse TU tagging: a chemical/genetic intersectional method for purifying cell type-specific nascent RNA. *Genes Dev* 2013; 27: 98–115.
21. Fernandez-Klett F, Offenhauser N, Dirnagl U, et al. Pericytes in capillaries are contractile in vivo, but arterioles mediate functional hyperemia in the mouse brain. *Proc Natl Acad Sci U S A* 2010; 107: 22290–22295.
22. Okabe M, Ikawa M, Kominami K, et al. ‘Green mice’ as a source of ubiquitous green cells. *FEBS Lett* 1997; 407: 313–319.
23. Khan MA, Schultz S, Othman A, et al. Hyperglycemia in stroke impairs polarization of monocytes/macrophages to a protective noninflammatory cell type. *J Neurosci* 2016; 36: 9313–9325.
24. Schneider A, Martin-Villalba A, Weih F, et al. NF-kB is activated and promotes cell death in focal cerebral ischemia. *Nat Med* 1999; 5: 554–559.
25. Dogbevia GK, Töllner K, Körbelin J, et al. Gene therapy decreases seizures in a model of Incontinentia pigmenti. *Ann Neurol* 2017; 82: 93–104.
26. Wenzel J, Hansen CE, Bettoni C, et al. Impaired endothelium-mediated cerebrovascular reactivity promotes anxiety and respiration disorders in mice. *Proc Natl Acad Sci U S A* 2020; 117: 1753–1761.
27. Müller-Fielitz H, Stahr M, Bernau M, et al. Tanycytes control the hormonal output of the hypothalamic-pituitary-thyroid axis. *Nat Commun* 2017; 8: 484.
28. Binder S, Baier PC, Molle M, et al. Sleep enhances memory consolidation in the hippocampus-dependent object-place recognition task in rats. *Neurobiol Learn Mem* 2012; 97: 213–219.
29. Patel J, Seppanen EJ, Rodero MP, et al. Functional definition of progenitors versus mature endothelial cells reveals key SoxF-dependent differentiation process. *Circulation* 2017; 135: 786–805.
30. Yu QC, Song W, Wang D, et al. Identification of blood vascular endothelial stem cells by the expression of protein C receptor. *Cell Res* 2016; 26: 1079–1098.
31. Li YF, Ren LN, Guo G, et al. Endothelial progenitor cells in ischemic stroke: an exploration from hypothesis to therapy. *J Hematol Oncol* 2015; 8: 33.
32. Körbelin J, Dogbevia G, Michelfelder S, et al. A brain microvasculature endothelial cell-specific viral vector with the potential to treat neurovascular and neurological diseases. *EMBO Mol Med* 2016; 8: 609–625.
33. Bergers G and Benjamin LE. Tumorigenesis and the angiogenic switch. *Nat Rev Cancer* 2003; 3: 401–410.
34. Kisseleva T, Song L, Vorontchikhina M, et al. NF-kB regulation of endothelial cell function during LPS-induced toxemia and cancer. *J Clin Invest* 2006; 116: 2955–2963.
35. Tabruyn SP and Griffioen AW. NF-kappa B: a new player in angiostatic therapy. *Angiogenesis* 2008; 11: 101–106.
36. Taniguchi K and Karin M. NF-kappaB, inflammation, immunity and cancer: coming of age. *Nat Rev Immunol* 2018; 18: 309–324.
37. Narayanan MJ, Rangasamy S and Narayanan V. Incontinentia pigmenti (Bloch-Sulzberger syndrome). *Handbook Clin Neurol* 2015; 132: 271–280.
38. Vanlandewijck M, He L, Mae MA, et al. A molecular atlas of cell types and zonation in the brain vasculature. *Nature* 2018; 554: 475–480.
39. Anderova M, Vorisek I, Pivonkova H, et al. Cell death/proliferation and alterations in glial morphology contribute to changes in diffusivity in the rat hippocampus after hypoxia-ischemia. *J Cereb Blood Flow Metab* 2011; 31: 894–907.
40. O’Donnell SL, Frederick TJ, Krady JK, et al. IGF-I and microglia/macrophage proliferation in the ischemic mouse brain. *Glia* 2002; 39: 85–97.
41. Li T, Pang S, Yu Y, et al. Proliferation of parenchymal microglia is the main source of microgliosis after ischaemic stroke. *Brain* 2013; 136: 3578–3588.
42. Hooper C, Taylor DL and Pocock JM. Pure albumin is a potent trigger of calcium signalling and proliferation in microglia but not macrophages or astrocytes. *J Neurochem* 2005; 92: 1363–1376.